CrystEngComm

View Online
Dynamic Article Links

Cite this: *CrystEngComm*, 2011, **13**, 4695

www.rsc.org/crystengcomm

PAPER

Influence of $ZnWO_4$ nanorod aspect ratio on the photocatalytic activity†

Di Li,[a] Rui Shi,[a] Chengsi Pan,[a] Yongfa Zhu*[a] and Huijun Zhao[b]

Received 27th February 2011, Accepted 15th April 2011
DOI: 10.1039/c1ce05256j

$ZnWO_4$ nanorod photocatalysts with various aspect ratios were synthesized by a hydrothermal method. The aspect ratio of the $ZnWO_4$ nanorods was governed by the hydrothermal temperature and pH value. $ZnWO_4$ nanorod photocatalysts showed highly efficient photocatalytic activity for the degradation of methylene blue under ultraviolet light irradiation. The photocatalytic activity and the effective separation of photogenerated electron–hole pairs were promoted by the increasing aspect ratio of the $ZnWO_4$ nanorods. The amount of electron donors in the $ZnWO_4$ increased with the aspect ratio of $ZnWO_4$, which was in good agreement with photocurrent results. The enhancement of photocurrent density and photocatalytic activity resulted from the reduction of charge-transfer resistance and capacitive reactance, which were deduced by the high aspect ratio of $ZnWO_4$ nanorods.

1. Introduction

$ZnWO_4$ has attracted a great deal of research attention due to its wide physical and chemical properties,[1–10] among which the photocatalysis properties have been extensively investigated.[11–20] Up to now, $ZnWO_4$ with different morphologies has been prepared, including porous $ZnWO_4$ films,[11,12] nanorods,[13] nanoparticles,[14] *etc.* It was believed that the difference in catalytic activities among these different morphologies of $ZnWO_4$ was mainly caused by their crystallinity and surface area. Our group has reported that the photocatalytic activity of $ZnWO_4$ was influenced by porous structure,[12] crystal growth orientation,[17] OH^- defects[18] and ion doping.[19] Besides, they have also reported a synergetic effect of enhancing catalytic activity in degrading RhB *via* combining electro-oxidation with photocatalysis.[13] However, work concerning the aspect ratio of the $ZnWO_4$ has not been reported. Therefore, there is a need to investigate the influence of the $ZnWO_4$ nanorod aspect ratio on the photocatalytic activity.

For one-dimensional nanostructured crystals the space charge region was well constructed along the longitudinal direction of the nanocrystal, meaning that photogenerated electrons could flow in the direction of the crystal length. Increased delocalization of electrons at one-dimensional nanostructured crystals could lead to a remarkable decrease in the e^-/h^+ recombination probability.[21] Consequently, larger numbers of e^- and h^+ existed on the active sites of the nanocrystal. So the investigation concerning the relationship between photocatalytic activity and the aspect ratio of one-dimensional nanostructured crystals was quite meaningful.[22]

In this work, the influence of aspect ratio of $ZnWO_4$ nanorods on the photocatalytic decomposition of methylene blue has been studied. The influence of the aspect ratio of $ZnWO_4$ nanorods was demonstrated by comparing the electrochemical behavior of each shape with photocatalytic activity in the oxidation of methylene blue.

2. Experimental section

2.1. Materials

Methylene blue was of analytical reagent grade quality used without further purification. Other chemicals were commercial products of analytical grade or reagent-grade. All the solutions were prepared with distilled water.

2.2. Preparation of $ZnWO_4$

In a typical synthesis procedure, $Na_2WO_4 \cdot 2H_2O$ (2 mmol) was dissolved in deionized water (14 mL) completely. Under vigorous agitation, an aqueous solution (14 mL) containing Zn $(NO_3)_2 \cdot 6H_2O$ (2 mmol) was added into the above solution at room temperature. The pH value of the mixture was adjusted with 10 M NaOH. Then, the mixture was transferred into a Teflon-lined steel autoclave of 40 mL and the autoclave was heated under autogenous pressure at a series of temperatures for 24 h. Afterward, the autoclave was cooled to room temperature gradually. The white precipitate was washed with distilled water three times. Then, it was dried at 60 °C in the open air.

2.3. Characterizations

The degradation rates of methylene blue (MB) solutions were scanned by a Hitachi U-3010 spectrophotometer periodically and the maximum absorption wavelength of the MB solution was identified at 664 nm. UV–vis spectra data were recorded in

[a]*Department of Chemistry, Tsinghua University, Beijing, 100084, China. E-mail: zhuyf@tsinghua.edu.cn*
[b]*Centre for Clean Environment and Energy and Griffith School of Environment Gold Coast Campus, Griffith University, QLD 4222, Australia*

† Electronic supplementary information (ESI) available. See DOI: 10.1039/c1ce05256j

the range from 200 to 800 nm. The pH value was measured by a Model PHSJ–4A pH meter. X-Ray diffraction (XRD) experiments were carried out using a Rigaku DMAX-2400 diffractometer with Cu-Kα radiation. The size and morphologies of $ZnWO_4$ and ZnO were characterized by the aid of a JEOL JEM-6700F field emission scanning electron microscope (SEM), LEO-1530 field emission scanning electron microscope and JEOL 2010F transmission electron microscope (TEM). The transient photoluminescence measurements were carried out using a steady state and time-resolved fluorescence/phosphorescence spectrometer (FLSP920, Edinburgh Instruments Ltd.). The Brunauer–Emmett–Teller (BET) surface area was measured by ASAP 2010 V5.02H.

2.4. Photo-electrochemical properties

Photo-electrochemical measurements were carried out using a conventional three-electrode, single-compartment glass cell fitted with a synthesized quartz window using a potentiostat. The quartz electrolytic cell was filled with 0.1 M Na_2SO_4. A total of 10 mg of synthesized $ZnWO_4$ was dropped on the ITO glass (2.0 $\times$ 4.0 cm), which was used as a working electrode for electrochemical impedance spectroscopy (EIS) and chronoamperometry experiments. Chronoamperometry was performed at a dc bias of 0.5 V. An 18 W germicidal lamp (λ = 254 nm, Institute of Electric Light Source, Beijing) was used as the light source for the UV light irradiation in the photoelectrochemical analyses. The counter and reference electrodes were a platinum black wire and saturated calomel electrode (SCE), respectively. The photoelectrochemical experiment was performed using an electrochemical system (CHI-660B, PR China).

2.5. Photocatalytic oxidative degradation

The photocatalytic activities of the $ZnWO_4$ were evaluated by the MB decomposition under ultraviolet irradiation. Ultraviolet light was obtained by a 12 W Hg lamp (λ = 254 nm, the Institute of Electric Light Sources, Beijing) and the average light intensity was 1 mW cm^{-2}. The radiant flux was measured with a power meter (the Institute of Electric Light Sources, Beijing).

The photocatalytic degradation of MB in the aqueous solutions was studied by using $ZnWO_4$ as the photocatalyst under room temperature and normal atmospheric pressure. $ZnWO_4$ (50 mg) and 100 ml MB (1×10^{-5} M) aqueous solution were added into the reactor, and then stirred with a magnetic stirrer prior to irradiation with Hg lamp at room temperature. After the reaction, the sample solution was put in a centrifuge to remove $ZnWO_4$ particles from solution. The solution obtained this way was extracted into a quartz cell. The absorbance of the samples was measured with quartz cells every 5 min.

3. Results and discussion

3.1. Controlling the synthesis of different aspect ratios of $ZnWO_4$ nanorods

3.1.1 Synthesis of $ZnWO_4$ nanorods. The pH value of the starting precipitate precursors had a crucial effect on formation of $ZnWO_4$. The precursor suspensions were adjusted to the desired pH values by adding NaOH solution, and then were hydrothermally treated at 160 °C for 24 h. Fig. 1 shows the XRD patterns of $ZnWO_4$ samples prepared by a hydrothermal procedure at different pH values. The diffraction peaks of all the samples could be easily indexed as a pure, monoclinic wolframite tungstate structure $ZnWO_4$, which was in good agreement with the standard card (JCPDS card number: 15-0774). Further increasing the pH value of the starting precipitate precursors to 8 resulted in the product containing another phase—ZnO (JCPDS card number: 036-1451). When the pH was adjusted to 10, the product was pure ZnO confirmed by its XRD pattern (Fig. 1).

The microstructures of the as-prepared samples were then investigated with SEM and TEM. Fig. 2a shows the SEM micrograph for the sample whose pH value was 5, and we could see that the samples were hollow spherical-like particles (Fig. 2a and 2b). It looked like that many $ZnWO_4$ particles were accumulated by self-assembly. As the pH value was adjusted to 6, all hollow spheres were transformed to small nanoparticles (Fig. 2c). When the pH value was increased to 7, all nanoparticles were evolved to nanorods with diameters of 10–20 nm and lengths of 100–150 nm (Fig. 2d). The microstructures of the as-prepared samples were then investigated with TEM. The HRTEM image (Fig. 2e) showed the interplanar spacing of nanorods was about 4.7 Å which coordinated with the XRD peak for the [100] plane (2θ = 30.5°), which revealed the nanorods preferred to grow along the [100] direction. When the pH was adjusted to 10, the product was pure ZnO which showed hollow spindles, as shown in Fig. 2f.

The $ZnWO_4$ nanorod formation was a typical hydrothermal ripening process:[5] a highly supersaturated solution was adopted, and amorphous fine particles acted as the precursor for the synthesis of crystallized $ZnWO_4$. At the beginning, the direct mixing of the two solutions led to the formation of a lot of amorphous fine particles (Fig. 3a). Under hydrothermal treatment, the formation of tiny crystalline nuclei in a supersaturated medium occurred. Then the crystal growth followed. The larger particles grew at the cost of the small ones, due to the energy difference in solubility between the large particles and the smaller particles, according to the well-known Gibbs–Thomson law.[23] In

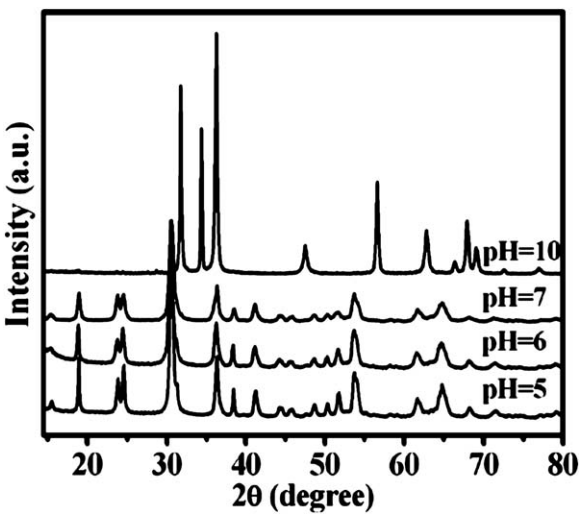

Fig. 1 XRD pattern: pH value series samples treated at 160 °C.

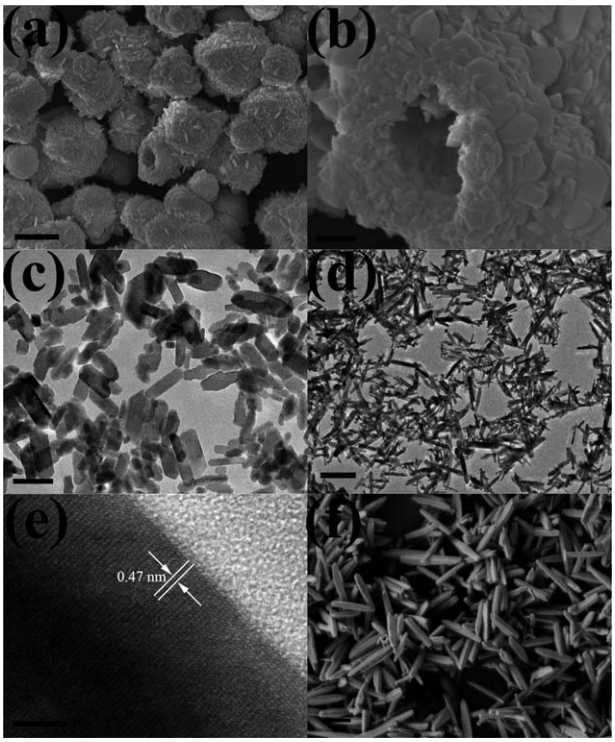

Fig. 2 SEM and TEM images (a) and (b) of $ZnWO_4$ hollow spherical-like particles; (c) $ZnWO_4$ nanoparticles; (d) $ZnWO_4$ nanorods; (e) HRTEM image of a single $ZnWO_4$ nanorod; (f) ZnO hollow spindles. Scale bar is 1 μm in (a), 200 nm in (b), 50 nm in (c), 200 nm in (d), 5 nm in (e) and 1 μm in (f).

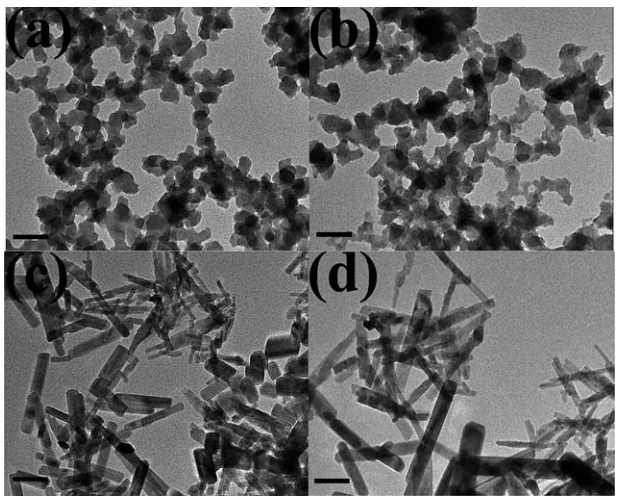

Fig. 3 Morphologies of time series samples treated at 160 °C: (a) 0, (b) 1, (c) 4, (d) 15 h. Scale bar is 50 nm in (a), 50 nm in (b) and 50 nm in (c) and (d).

the early stages, an examination of the intermediate samples showed the coexistence of short rod structures and irregular nanoparticles (Fig. 3c). As the reaction continued, irregular nanoparticles and short nanorods vanished, and larger nanorods formed, suggesting that the nanorods grew at the cost of the smaller particles and rods (Fig. 3d).[24,25] The XRD patterns of time series samples treated at 160 °C accorded with TEM, the $ZnWO_4$ crystalline phase appeared only after 4 h hydrothermal treatment (Fig. 4). When the $ZnWO_4$ crystalline phase appeared, the particles appeared at the same time.

3.1.2 Effects of temperature on the aspect ratio of $ZnWO_4$ nanorods. The temperature had a significant effect on the aspect ratio of $ZnWO_4$ nanorods. Fig. 5a–5e show the morphologies of temperature series samples prepared in various temperature hydrothermal conditions at pH = 7. On the basis of TEM images, it could be found that the higher temperature treatment produced longer nanorods, and the length of $ZnWO_4$ nanorods increased from 100 nm to 500 nm. The aspect ratios of $ZnWO_4$ nanorods at different temperatures are shown in Fig. 5f. Fig. 5f shows that the aspect ratio of $ZnWO_4$ nanorods increased with the increasing temperature. So the hydrothermal temperature was the key factor of controlling the aspect ratio of $ZnWO_4$ nanorods.

3.1.3 Formation mechanism of different aspect ratios of $ZnWO_4$ nanorods. On the basis of the experimental results, we proposed that the evolution of phase composition during hydrothermal synthesis of $ZnWO_4$ in neutral conditions was a dynamic process which occurs under the influence of the kinetic factors,[26] from small nanoparticles to nanorods. As the temperature increased, the diffusion rate of the atom located on the nanorod's surface increased. Due to the larger surface atom ratio of smaller nanorods, the influence of increasing temperature was more obvious on smaller nanorods which were less stable. So the reaction system was favorable for the formation of larger aspect ratio $ZnWO_4$ nanorods along with increasing temperature.

3.2. Effects of aspect ratio of $ZnWO_4$ nanorods on the photochemical and electrochemical properties

Electrochemical impedance spectroscopy (EIS) was used to characterize electrochemical interfacial reactions. The photocatalytic decomposition of MB could be explained as an electrochemical oxidation reaction in which reactants supply electrons to an anode. Fig. 6 shows the EIS response of $ZnWO_4$

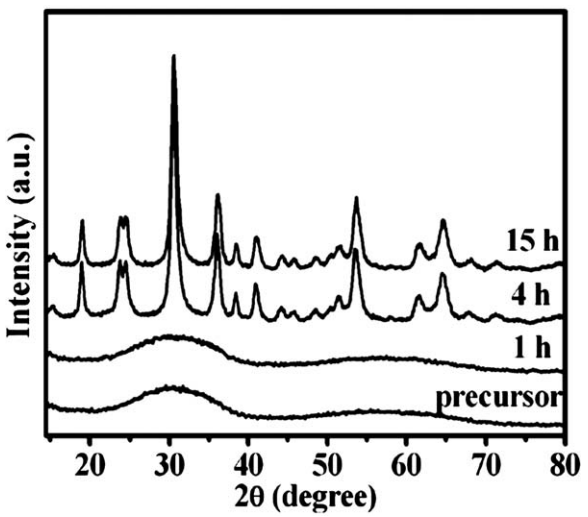

Fig. 4 XRD pattern: time series samples treated at 160 °C.

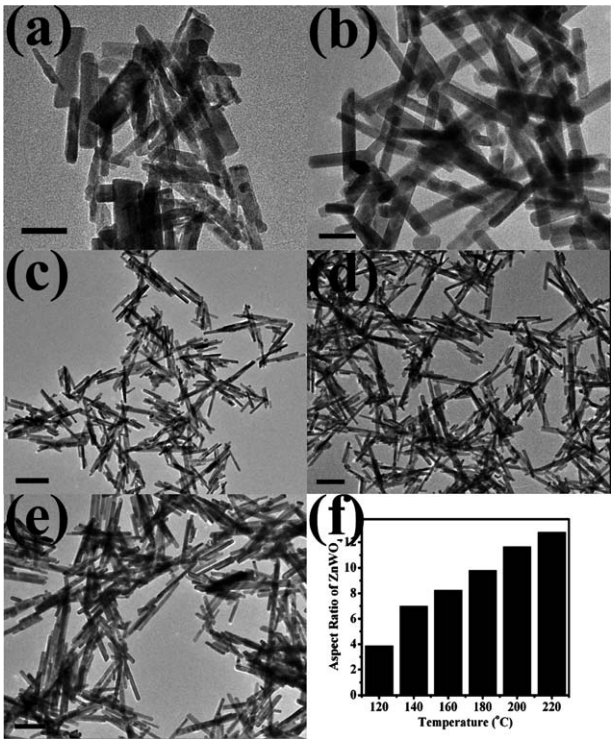

Fig. 5 Morphologies of temperature series $ZnWO_4$ samples: (a) 120 °C, (b) 140 °C, (c) 180 °C, (d) 200 °C, (e) 220 °C; (f) the aspect ratio of $ZnWO_4$ nanorods obtained at different temperatures. Scale bar is 50 nm in (a), 50 nm in (b) and 200 nm in (c), (d) and (e).

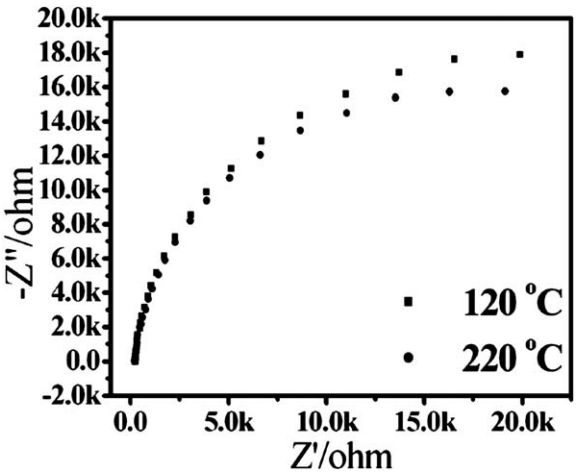

Fig. 6 The EIS response of $ZnWO_4$ under ultraviolet light irradiation (λ = 254 nm).

nanorod under ultraviolet light irradiation (λ = 254 nm). The radius of the arc on the EIS Nyquist plot reflects the reaction rate occurring at the surface of the electrode. The radii tended to decrease significantly with the increasing aspect ratio of the $ZnWO_4$ nanorods, indicating that both charge-transfer resistance and capacitive reactance decreased with increasing aspect ratio. It suggested that there was an effective separation of photogenerated electron–hole pairs and that fast interfacial charge transfer to the electron donor/electron acceptor occurred, as suggested by Leng *et al.*[27] The electron-transfer rate from electrolyte to the electrode surface was enhanced in $ZnWO_4$ nanorods, for which photogenerated electrons could easily flow to the bulk electrode because the space charge region was well developed along the longitudinal direction of the nanorods. This led to a reduction in the probability of e^-/h^+ recombination; consequently, the large number of holes on the surface could induce electron movement toward the electrode, resulting in an enhancement in the photocatalytic oxidation rate and affecting the capacitive reactance. The aspect ratio of the $ZnWO_4$ was also evaluated by the photocurrent. It could be seen that the photocurrent was enhanced along with the aspect ratio of $ZnWO_4$. The lifetime of e^- and h^+ on the active site under illumination increased with the increasing aspect ratio of $ZnWO_4$ due to a reduction in e^-/h^+ recombination probability. The greater number of electron donors at longer nanorods led to an increase in the current flow rate (Fig. 7). Fig. 8 gives room temperature time-resolved transient photoluminescence decays of $ZnWO_4$ nanorods of different aspect ratios. The photoluminescence lifetime of $ZnWO_4$ nanorods was on the order of nanoseconds, and the photoluminescence lifetime of $ZnWO_4$ nanorods increased with increasing aspect ratio: 220 °C (66.92 ns) > 120 °C (60.55 ns). It meant there were more e^- and h^+ on the active site under illumination when the largest aspect ratio $ZnWO_4$ nanorods were used as catalysts.

3.3. Effects of aspect ratio of $ZnWO_4$ nanorods on photocatalytic activity

Based on the experimental procedures described above, the photocatalytic degradation of MB in aqueous solutions was investigated under ultraviolet light irradiation (λ = 254 nm). The characteristic absorption of MB at 664 nm was chosen as the monitored parameter for the photocatalytic degradation process. Fig. 9 shows the degradation of MB using temperature series $ZnWO_4$ samples. The first-order linear relationship was revealed by the plots of the $\ln(C/C_0)$ *vs.* irradiation time (t), where C was the concentration of MB at the irradiation time t and C_0 was the concentration in the adsorption equilibrium of the photocatalysts before irradiation. *Via* the first order linear fit, the determined reaction-rate constants k were 0.07348, 0.08618,

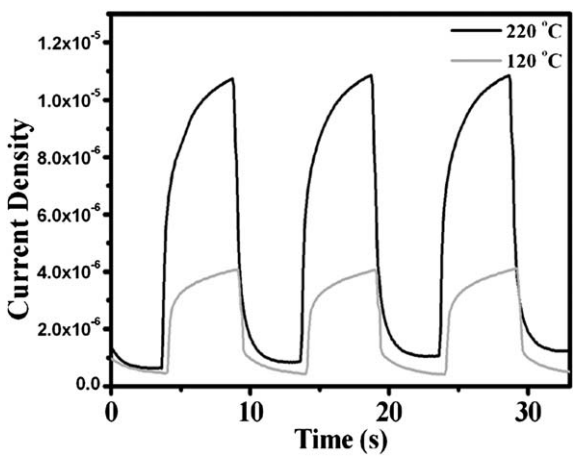

Fig. 7 Current density transient with light on/off every 5 s for $ZnWO_4$.

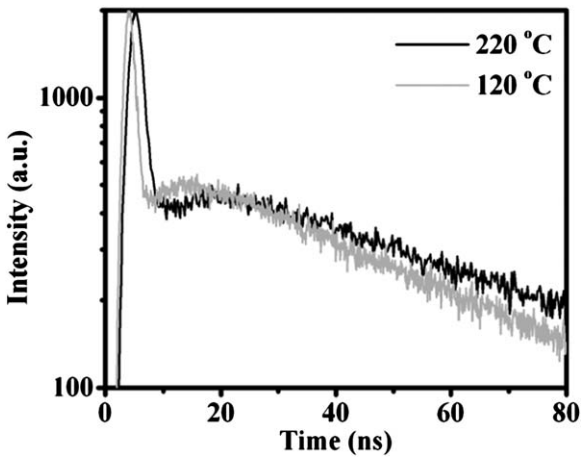

Fig. 8 Room temperature time-resolved transient photoluminescence decays for the $ZnWO_4$ nanorods, excited at 254 nm.

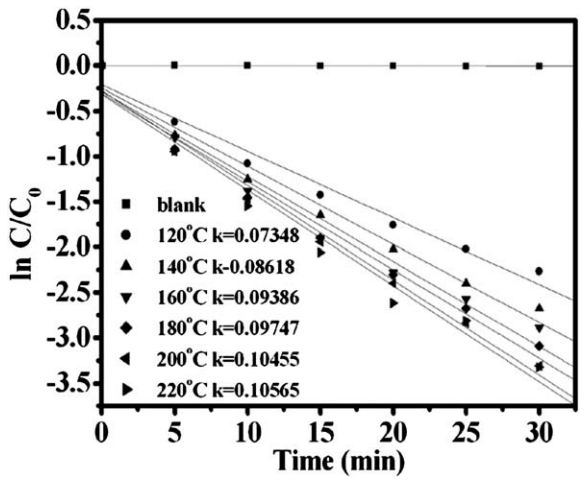

Fig. 9 First-order plots for the photocatalytic degradation of MB using various $ZnWO_4$ samples: temperature series samples.

0.09386, 0.09747, 0.10455 and 0.10565 min^{-1}, respectively, for the aspect ratio series samples. The photocatalytic activity heightened as the aspect ratio increased. As can be seen from Fig. 9, the MB solution could be stably reserved under the irradiation of ultraviolet light. The concentration of MB was decreased sharply by $ZnWO_4$ nanorods. Large numbers of photogenerated e^-/h^+ pairs on the surface of $ZnWO_4$ nanorods led to the rapid oxidation of MB. Photo-generated electrons and holes within the $ZnWO_4$ nanorods either took part in the redox reactions at the surface or recombined. The recombination process had faster kinetics than the redox reactions and therefore controls the efficiency of the photocatalytic process.[28] In the presence of $ZnWO_4$ nanorods, the space charge region was well developed along the longitudinal direction of nanorods. This led to a reduction in the probability of e^-/h^+ recombination; consequently, the possibility of the recombination of e^-/h^+ pairs decreased with increasing aspect ratio. Meanwhile, O_2 absorbed on the surface of the $ZnWO_4$ nanorods could accept e^- and form O_2^- which then oxidizes MB directly on the surface.[29] As shown

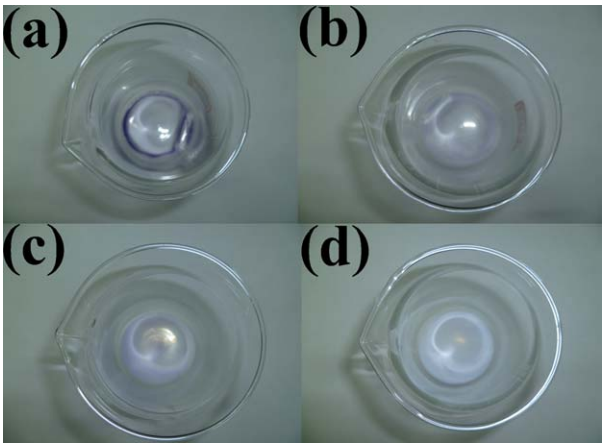

Fig. 10 Photographs of temperature series $ZnWO_4$ samples after the photocatalysis reaction finished: (a) 160 °C; (b) 180 °C; (c) 200 °C; (d) 220 °C.

in Fig. 10, MB absorbed by the $ZnWO_4$ nanorod surface decreased sharply with increasing hydrothermal temperature. Besides MB, $ZnWO_4$ nanorod photocatalysts also showed highly efficient photocatalytic activity for the degradation of phenol (Fig. S1, ESI†). The surface area of $ZnWO_4$ nanorods decreased with increasing aspect ratio: 220 °C (21 m^2 g^{-1}) < 120 °C (40 m^2 g^{-1}). It meant that surface area had no obvious effect on the photocatalytic degradation of MB in aqueous solutions. As a result, the aspect ratio played a very important part in the photocatalytic activity and photocurrent.

4. Conclusions

In conclusion, the photocatalytic properties of $ZnWO_4$ nanorods were investigated under ultraviolet light irradiation in detail. The effective separation of photogenerated electron–hole pairs and fast interfacial charge transfer to the electron donor/electron acceptor were enhanced with increasing aspect ratio of the $ZnWO_4$ nanorods. A decrease in the probability of e^-/h^+ recombination led to an increase in electron donors at longer $ZnWO_4$ nanorods. Consequently, photocatalytic activity was highest when the largest aspect ratio $ZnWO_4$ nanorods were used for the photocatalytic decomposition of MB.

Acknowledgements

This work is supported by Chinese National Science Foundation (20925725 and 50972070) and National Basic Research Program of China (2007CB613303).

Notes and references

1 T. Oi, K. Takagi and T. Fukazawa, *Appl. Phys. Lett.*, 1980, **36**, 278.
2 V. Nagirnyi, M. Kirm, A. Kotlov, A. Lushchik and L. Jonsson, *J. Lumin.*, 2003, **13**, 639.
3 S. Nedilko, Y. Hizhnyi and T. Nikolaenko, *Phys. Status Solidi C*, 2005, **2**, 481.
4 A. Watterich, L. A. Kappers and O. R. Gilliam, *Solid State Commun.*, 1997, **104**, 683.
5 S. H. Yu, B. Liu, M. S. Mo, J. H. Huang, X. M. Liu and Y. T. Qian, *Adv. Funct. Mater.*, 2003, **13**, 639.
6 X. Cao, W. Wu, N. Chen, Y. Peng and Y. Liu, *Sens. Actuators, B*, 2009, **137**, 83.

7 T. Montini, V. Gombac, A. Hameed, L. Felisari, G. Adami and P. Fornasiero, *Chem. Phys. Lett.*, 2010, **498**, 113.
8 S. J. Chen, J. H. Zhou, X. T. Chen, J. Li, L. H. Li, J. M. Hong, Z. Xue and X. Z. You, *Chem. Phys. Lett.*, 2003, **375**, 185.
9 P. Siriwong, T. Thongtem, A. Phuruangrat and S. Thongtem, *CrystEngComm*, 2011, **13**, 1564.
10 J. H. Pan, H. Dou, Z. Xiong, C. Xu, J. Ma and X. S. Zhao, *J. Mater. Chem.*, 2010, **20**, 4512.
11 X. Zhao and Y. F. Zhu, *Environ. Sci. Technol.*, 2006, **40**, 3367.
12 X. Zhao, W. Q. Yao, Y. Wu, S. C. Zhang, H. P. Yang and Y. F. Zhu, *J. Solid State Chem.*, 2006, **179**, 2562.
13 H. B. Fu, J. Lin, L. W. Zhang and Y. F. Zhu, *Appl. Catal., A*, 2006, **306**, 58.
14 G. L. Huang, C. Zhang and Y. F. Zhu, *J. Alloys Compd.*, 2007, **432**, 269.
15 G. L. Huang and Y. F. Zhu, *J. Phys. Chem. C*, 2007, **111**, 11952.
16 W. Zhao, X. Y. Song, G. Z. Chen and S. X. Sun, *J. Mater. Sci.*, 2009, **44**, 3082.
17 R. Shi, Y. J. Wang, D. Li, J. Xu and Y. F. Zhu, *Appl. Catal., B*, 2010, **100**, 173.
18 J. Lin, J. Lin and Y. F. Zhu, *Inorg. Chem.*, 2007, **46**, 8372.
19 G. L. Huang, S. C. Zhang, T. G. Xu and Y. F. Zhu, *Environ. Sci. Technol.*, 2008, **42**, 8516.
20 D. He, X. Zhang, T. Xie, J. Zhai, H. Li, L. Chen, L. Peng, Y. Zhang and T. Jiang, *Appl. Surf. Sci.*, 2011, **257**, 2327.
21 H. J. Yun, H. Lee, J. B. Joo, W. Kim and J. Yi, *J. Phys. Chem. C*, 2009, **113**, 3050.
22 L. Bauer, N. S. Birenbaum and G. J. Meyer, *J. Mater. Chem.*, 2004, **14**, 517.
23 J. W. Mullin, *Crystallization*, 3rd edn, Butterworth-Heinemann, Oxford, UK, 1997.
24 C. B. Murray, D. J. Norris and M. G. Bawendi, *J. Am. Chem. Soc.*, 1993, **115**, 8706.
25 H. Zhang, L. Wang, H. Xiong, L. Hu, B. Yang and W. Li, *Adv. Mater.*, 2003, **15**, 1712.
26 A. Testino, I. R. Bellobono, V. Buscaglia, C. Canevali, M. D'Arienzo, S. Polizzi, R. Scotti and F. Morazzoni, *J. Am. Chem. Soc.*, 2007, **129**, 3564.
27 W. H. Leng, Z. Zhang, J. Q. Zhang and C. N. Cao, *J. Phys. Chem. B*, 2005, **109**, 15008.
28 M. R. Hoffmann, S. T. Martin, W. Y. Choi and D. W. Bahnemann, *Chem. Rev.*, 1995, **95**, 69.
29 L. W. Zhang, H. B. Fu and Y. F. Zhu, *Adv. Funct. Mater.*, 2008, **18**, 2180.

